

Learning image from projection: a full-automatic reconstruction (FAR) net for sparse-views computed tomography

Genwei Ma, Yining Zhu*, *Member, IEEE*, Xing Zhao

Abstract—The sparse-views x-ray computed tomography (CT) is essential for medical diagnosis and industrial nondestructive testing. However, in particular, the reconstructed image usually suffers from complex artifacts and noise, when the sampling is insufficient. In order to deal with such issue, a full-automatic reconstruction (FAR) net is proposed for sparse-views CT reconstruction via deep learning technique. Different with the usual network in deep learning reconstruction, the proposed neural network is an end-to-end network by which the image is predicted directly from projection data. The main challenge for such a FAR-net is the space complexity of the CT reconstruction in full-connected (FC) network. For a CT image with the size $N \times N$, a typical requirement of memory space for the image reconstruction is $O(N^4)$, for which is unacceptable by conventional calculation device, e.g. GPU workstation. In this paper, we utilize a series of smaller FC layers to replace the huge layer based on the sparse nonnegative matrix factorization (SNMF) theory. By applying such an approach, the FAR-net is able to reconstruct sparse-views CT images with the size 512×512 on only single workstation. Furthermore, an artifact suppression neural network (AS-NN) structure is composed in the FAR-net for suppressing the artifacts and noise caused by under-sampling data. The results of numerical experiments show that the projection matrix and the FAR-net is able to reconstruct the CT image from sparse-views projection data with a superior quality than conventional methods such as FBP and optimization based approach. Meanwhile, the factorization for the inverse projection matrix is validated in numerical.

Index Terms—deep learning, sparseness non-negative matrix factorization, Full-automatic reconstruction, sparse-views CT

I. INTRODUCTION

X-ray computed tomography (CT) has been widely used in medical diagnostic and industrial nondestructive testing due to its great ability in visualizing interior structure. Considering the damage of radiation to patients, it is of great significance and essential to reduce the dose in the practical application. One of the effective methods to reduce the dose is to decrease the scanning angles which be named sparse-views CT. However, the sparse-views scanning will lead in a variety of issues in reconstructed images such as artifacts and noise. Many studies have demonstrated that the traditional

methods [1], such as filter back-projection (FBP), algebraic reconstruction algorithm (ART) [2], simultaneous algebraic reconstruction technique (SART) [3], expectation maximization (EM) [4], are failed to deal with these issues via theories or experiments. In order to improve the quality of reconstructed images from sparse-views scanning, various methods have been proposed according to compressive sensing (CS) theory [5]. Most of them are based on optimization model which imports some prior knowledge as constraints terms. For example, some studies utilize L_1 regularization term of the gradient of images for dealing with different issues, such as sparse-views, low-dose, limited-angle as well as interior tomography. Such type of regularization is also named as Total variation (TV) [6]–[9] which is based on the assumption that the gradient of CT images is sparse. Inspired by the sparsity of image, many approaches are proposed e.g. dictionary learning [10], non-local means (NLM) [11]–[13] and different wavelet transform methods [14] [15]. These approaches prove satisfied results in varying degrees for removing artifacts and suppressing noise. However, it still remain two main barriers for applying the approach to practical application: the great computation cost caused by the iterative manner of the solving algorithm [16] and the difficulty of choosing the regularization parameters. Hence, it would be desperately desire for an approach with low complicated of computation and convenient parameter choosing in practical application.

Recently, deep learning technology has been applied in many fields with remarkable results which is benefited from dramatic improvements in CUDA acceleration [17]. In the field of CT image processing, there are various convolution neural network (CNN) and recurrent neural network (RNN) been proposed for image restoration [18] [19], denoising, artifacts correction [20] [21], low-dose CT [22]–[25], sparse-views CT [26] and spectral CT [27] in image domain. Furthermore, researchers began to incorporate iterative method into CNN [28] [29]. Although the results reported so far are remarkable in terms of image quality, these methods and the corresponding CNN frame can only be utilized in image domain, which is post-processing without achieving the stage of image reconstruction. In other words, these methods are semi-traditional and semi-deep learning. However, a deep network mimics an organism better than a linear operator, and is much more intelligent than a linear system solver [30] as well. Hence, in practice, it is of great importance to build a end-to-end network which try to translate an image in a modality that is difficult to understand to a corresponding image which can

This work was partly supported by the National Natural Science Foundation of China (grants: 61827809, 61671311, 61501310, 61371195), Beijing Commission of Education grant KM201710028002.

G. Ma, Y. Zhu, X. Zhao are with school of Mathematical Sciences, Capital Normal University, Beijing, 100048, China, and with Beijing Advanced Innovation Center for Imaging Technology, Capital Normal University, Beijing, 100048, China. e-mail: (MaGenwei@126.com, ynzhu@cnu.edu.cn, zhaoxing_1999@126.com).

Y. Zhu serves as the correspondence author (e-mail: ynzhu@cnu.edu.cn).

be recognized by human [31] [32]. Würfl *et al.* have already demonstrated that image reconstruction can be expressed in term of neural network and shown that FBP can be mapped identically onto a deep neural network architecture [33]. In this method, the parameters of fully connected (FC) layer of neural network are fixed and pre-calculated by discrete formulation of FBP algorithm and the parameters of convolution layer are initialized by Ram-Lak filter. Argyrou *et al.* proposed an approach of artificial neural network reconstruction, and Zhu *et al.* show that sensor domain to image domain via automated transform by manifold approximation (AUTOMAP) [34]. Such neural network require an impractical amount of memory space which hamper the approach applied to practical. More specifically, the proposed neural network needs to train huge amount of parameters. The space complexity the of the network parameters is $O(n^4)$, where n is the width or height of reconstruction image. Because of memory limitation, the scheme can only reconstruct low resolution images. For example, if we want to reconstruct an image with a resolution of 512×512 using AUTOMAP method, the number of parameters (single float) is 512^4 , requiring 1 TB memory for which will be a heavy cost of computational hardware cost such as GPU. Li *et al.* proposed iCT-Net for CT images from sinogram data [35], which achieve back projection by introducing a fixed and separated rotation layer which is calculated based on the CT system's configuration. By this strategy, the size of mapped network could decrease dramatically.

In this paper, in order to take advantage and overcome shortcomings of end-to-end neural network for image reconstruction, we propose an approach to reduce the size of the FC layer based on the idea of sparseness non-negative matrix factorization (SNMF) [36]. Non-negative matrix factorization (NMF) is usually utilized for parts-based representations in machine learning [37] in earlier study. For a given non-negative data matrix V , NMF finds an approximate factorization $W \approx V \cdot H$ into non-negative factors V and H [38]. Especially, if we make sparseness constraints at the matrix, the better quality will be achieved for NMF. By applying the SNMF idea, the space complexity of the network has been reduced to $O(n^3)$ and the requirement of the memory space has been decreased to an acceptable size. For example, we are even able to reconstruct CT image with a resolution of 512×512 for sparse-view scanning in a single workstation with multi-GPUs. Moreover, we integrate an artifact suppression neural network (AS-NN) to our network for furtherly suppressing the residual artifacts and noise caused by the sparse-views scanning. Hence, our network would learn features from data and reconstruct image without manual intervention and we name it as Full-Automatic Reconstruction (FAR) net. The numerical experiments show that FAR-net could be implemented on only one workstation and predict the CT image from projection data directly with a superior quality than traditional algorithm such as TV based approach.

The remain of the paper is organized as follows: the section II introduce related knowledge of CT as well as neural network including FC network and CNN. In the section III, we describe the proposed FAR-net which contains two strategies: reconstruction and artifacts suppression. In the section IV, numerical

experiments are carried out to verify the CT problem can map into FC network in low dimensions, but also is useful for sparse-views CT problem by two neural network. Finally, we summarize the paper in section V.

II. PRELIMINARY KNOWLEDGE

A. CT imaging

In ideal condition, the mathematical model of CT is usually described as a discrete linear system [39]

$$AX = b \quad (1)$$

where $A \in \mathbb{R}^{M \times N}$ denotes the projection matrix, \mathbf{x} denotes the reconstructed image and b denotes the projection data. It is an inverse problem for solving \mathbf{x} from b . For such a problem, it is difficult to obtain \mathbf{x} directly since the system matrix A is too huge to find the inverse matrix. Here the system matrix is $A_{(u \times v) \times (w \times h)} \triangleq A_{M \times N}$ where u, v are the number of detector bins and scanning samples, and w, h are the size of reconstruction image. It is noteworthy that A would be a typical sparse non-negative matrix and the size of would achieve about $2^{18} \times 2^{15}$ for a typical medical image.

B. Neural network

In recent years, the deep neural network (NN) has sprung up rapidly and is widely used in classification, object detection [40], [41], image segmentation [42], [43] and so on. Fully connection neural network (FCLs) and convolutional neural network (CNN) are two typical deep neural network. In this subsection, we will introduce the principle of these two networks.

1) *Fully connection neural network*: As shown in Fig. 1, the k -th layer ($X = (x_1, x_2, \dots, x_M)^T$) has M neurons and the $(k+1)$ -th layer ($Y = (y_1, y_2, \dots, y_N)^T$) has N neurons. So the weight matrix (W) of the two adjacent fully connected layers is a $M \times N$ matrix. A FCL can be described as Eq. (2):

$$Y = f(W \cdot X + b) \quad (2)$$

where f is the activation function and b is the bias. Without considering the bias and activation function, a FCL can be expressed as

$$Y = W \cdot X. \quad (3)$$

which is very similar to Eq. (1).

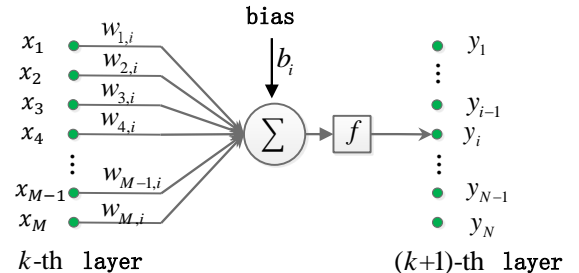


Fig. 1. A fully-connected layer between k -th layer and $(k+1)$ -th layer.

2) *Convolutional neural network*: Various types of CNNs have been proposed such as ResNet [44], U-net [43], DenseNet [45]. The simplest form of CNNs with n layers is expressed as

$$Y = f_n(BN(W_n * f_{n-1}(\cdots (W_2 * f_1(BN(W_1 * X + b_1) + b_2)) \cdots) + b_n)) \quad (4)$$

where X is the input data, W_i is the convolution kernel of the i -th layer, b_i is the bias of the i -th convolution layer, f_i is an activation function, $*$ is represented the convolution operation, BN denotes batch normalization and Y is output data or prediction. The goal of CNN framework is to find optimal parameters $W_i, b_i (i = 1, 2, \cdots, n)$ to minimize the following energy function,

$$E = \|Y^* - Y\|_{L_p} \quad (5)$$

where Y^* is the ground truth data and L_p is norm to measure the difference between the predicted result and the real data.

III. METHOD

As mentioned above, it is an enormous challenge to reconstruct CT image from projection data via a deep neural network without any manual intervention due to the unacceptable requirement of memory space. In this section, inspired by the matrix factorization, we propose a Full-Automatic Reconstruction (FAR) net to predict CT image from sparse-view projection data directly on a single workstation. The FAR-net is motivated by the following observations:

- the sparse matrix can be decomposed into the product of a series of matrices approximately based on SNMF theory;
- sparse-views CT images usually suffer from heavy artifacts and noise, and CNNs has great potential to remove such artifacts and noisy;
- a deep neural network is ideal to capture various types information from a large amount of training data [23].

Hence, we designed the FAR-net to provide two functions including image reconstruction image and artifacts suppression via FCLs and CNNs.

A. Reconstruction Neural Network

According NMF theory [36], a given non-negative matrix (W) can be factorized as follow:

$$W_{M \times N} \approx V_{M \times c} H_{c \times N} \quad (6)$$

where $c < \min(M, N)$ and both $V_{M \times c}$ and $H_{c \times N}$ are non-negative. To improve the quality of approximation of Eq. 6, there are different cost functions such as L_2 norm or Kullback-Leibler divergence:

$$E_{L_2} = \|VH - W\|_2^2, \quad (7)$$

$$E_{KL} = \sum_{ij} [(VH)_{ij} \log \frac{(VH)_{ij}}{W_{ij}} - (VH)_{ij} + W_{ij}]. \quad (8)$$

Lee *et al.* have found an algorithm to minimize E_{L_2} and E_{KL} and gave the proof of convergence [37]. Furthermore, Hoyer *et al.* indicated explicitly that incorporating the sparseness as

contrast for matrix could improve the result of factorization [36]. If we decompose V and H continually, the theory still works since both of them are SNMF. Hence, we could factorize the SNM within a few steps, e.g. 2 or 3 layers. Then, considering the huge projection matrix A in Eq.1, it could be approximatively represented by a series of smaller SNMs as follows,

$$A \approx V_1 \cdots V_n \cdot H_1 \cdots H_n. \quad (9)$$

In particular, the CT reconstruction can be considered as two processes: filter and back projection (FBP). The process of back projection also can be regarded as a linear transformation, and the sparse property of this linear transformation matrix R is consistent with the projection matrix A . The process of filter can be realized by convolution layer. Hence, we are able to learn the inverse of R based on Eq. 9 via FCLs neural network which are composed by some smaller middle layers. As shown in Fig. 2, these middle layers can effectively reduce the amount of network parameters and the requirement of memory space. Based on such a structure, we proposed the reconstruction neural network shown in Fig. 3 (Recon-NN). Although Eq. 9 is not strictly proofed in theory, numerical experiments indicate that the weights matrices of trained network is approximately enough equal to the inverse matrix. Therefore, the network is able to predict the CT image from projection data directly.

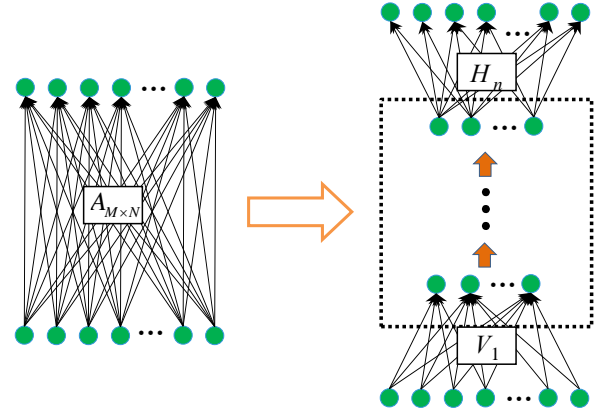


Fig. 2. Mapping matrix factorization into FC network. A inverse of SNM can be factor as some smaller matrix.

B. Artifacts suppression neural network

Generally speaking, sparse-views CT images usually suffer from complex artifacts as well as noise. In order to solve this issue, we propose an artifacts suppression neural network (AS-NN) to improve the quality of image which is predicted from Recon-NN. As you can see in Fig. 4, our network takes full advantage of residual block [44] and U-net architecture [43]. More specifically, the residual block are shown in the lower left corner of the Fig. 4. The bypass connections in the residual block is able to recover image with higher quality and to avoid vanishing gradient problem in back-propagating. Similarly, The U-net architecture also can preserves the details of high-frequency features. Since a typical CNN has pooling layers, the information may be lost after passing these layers.

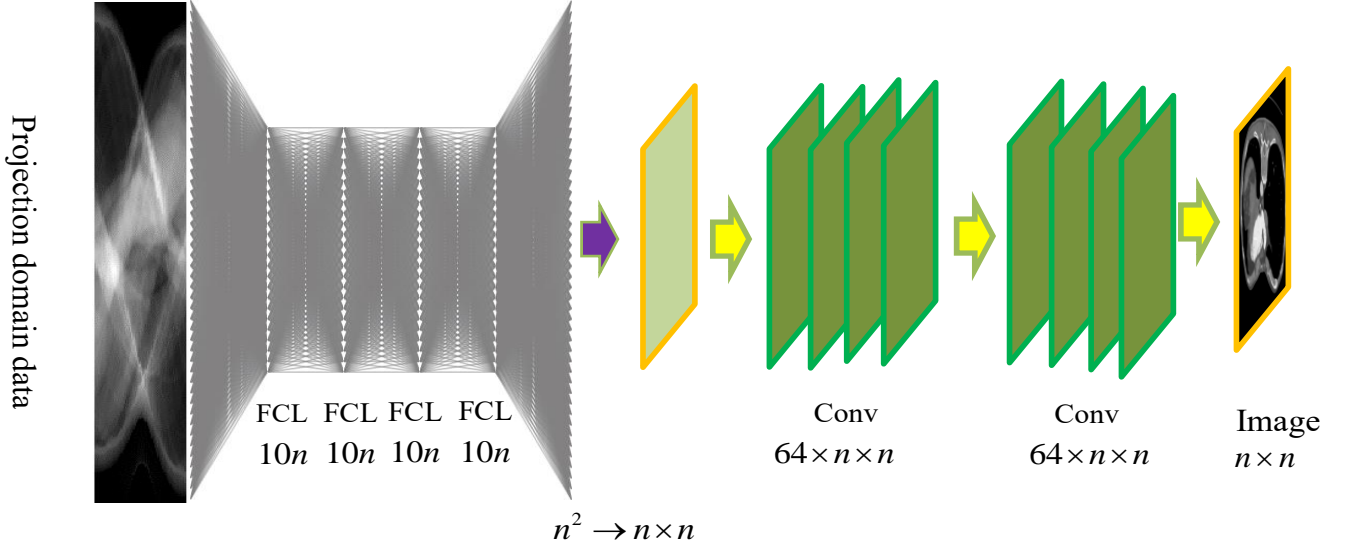


Fig. 3. Recon-NN frame for image reconstruction strategy. There are two parts in the frame. The first part consist five FC layers and the second part include three convolutional layers.

To avert this phenomenon, high-frequency features from the contracting path are combined with up-sampled output to recover the details [23]. In addition, our network has added its own features. Firstly, our network performs down-sampling and up-sampling on different scale spaces to realize information exchange in different scale spaces, while U-net has less communication between data in different scale spaces, and there is only one down-sampling and up-sampling in adjacent scales. Secondly, the information contained in different scale spaces is different. The space with larger resolution should contain more information, The space with larger resolution should contain more information, and the network should be set deeper. The number of convolution layers of our network for different scale spaces is different, while unet is the same different scale spaces.

In summary, as shown in Fig. 5, the FAR-net is an end-to-end network, which is composed of Recon-NN and AS-NN. Though pre-training is not required for the FAR-net, it could be considered as two steps: in the first step (Recon-NN), the FAR-net predict the CT image from input sparse-views projection data directly with artifacts and noise. Then the CT image are processed by the second step of FAR-net (AS-NN) to improve the image quality.

IV. NUMERICAL EXPERIMENTS

In this section, various experiments are carried to evaluate the FAR-net as well as the matrix factorization.

A. Validation of matrix factorization

We first perform some numerical experiments to validate the Equation (9). In order to simplify problem, we remove the convolution layers of Recon-NN in the testing (only FC network remained). However, it is difficult to estimate directly whether the predicted matrix which is defined as \hat{A} is inverse of A . So we calculate $E \approx W_k \cdots W_2 \cdot W_1 \cdot A = \hat{A}A$ as the

TABLE I
THE CONFIGURATION OF FC NETWORK

hardware	CPU	E5-2620 v3 $\times 2$
	GPU	NVIDIA GTX1080Ti
software	memory	512GB
	language	python3.6
	deep learning frame	pytorch0.4.0
hyper parameters	CUDA version	cuda9.1, cudnn7.1
	batch size	3000
	learning rate	0.0001
	optimizer	adam

evaluation objective, which should be equal or approximately equal to identity matrix (I). To train and validation the FC network (the simple version of Recon-NN), we have to prepare a large dataset comprising pairs of input data and label data. Firstly, we generate a nonnegative sparse matrix $A_{N \times N}$ randomly, of which the sparsity is $\frac{2\sqrt{N}}{N}$. Then, we select 100 images from Pascal VOC [46] and resize them to $N \times N$. Each row (X_i) of image can be regarded as ground truth data and $b_i (= A \cdot X_i)$ can be regraded as input data. Hence, the total number of training and testing data pairs is $100 \times N$. It is should be noticed that the operator is only a matrix multiplication rather than radon transform in this experiment. The configuration of the FC network is displayed in Table I.

In this testing, there are 4 aspects are studied for the impact of FC network in FAR-net: the depth of network, whether using nonnegative constraint (rectified linear unit activation function), the times of back-propagation and the dimension of A . Hence, we testing different matrix dimension and configurations of FC network. The results show that the inverse of the SNM is able to trained by the FC neural network with several smaller layers, and the dimension of corresponding matrices are much smaller than the inverse matrix. Furthermore, we can conclude some rules as follows:

- Fig. 6 shows loss curves with different number of middle

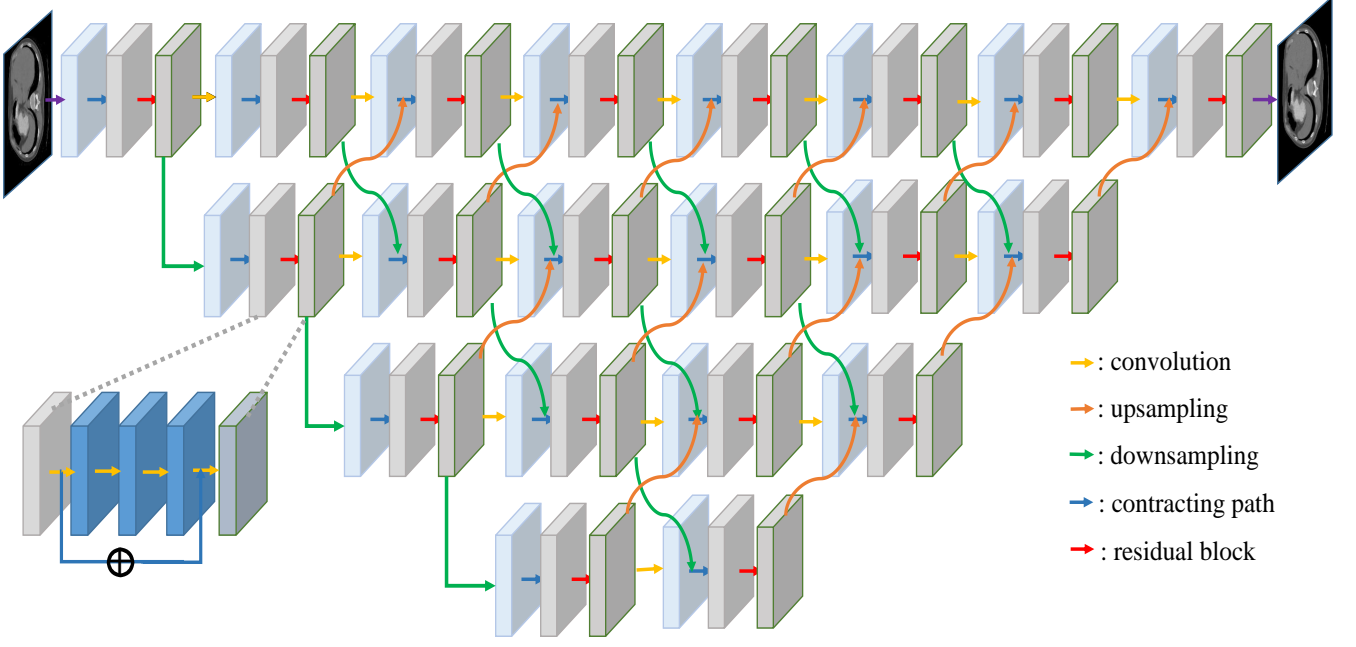


Fig. 4. AS-NN frame for artifact suppression and de-noising. The red arrow correspond to residual blocks and different scales of space are merged by convolution, up-sampling and down-sampling

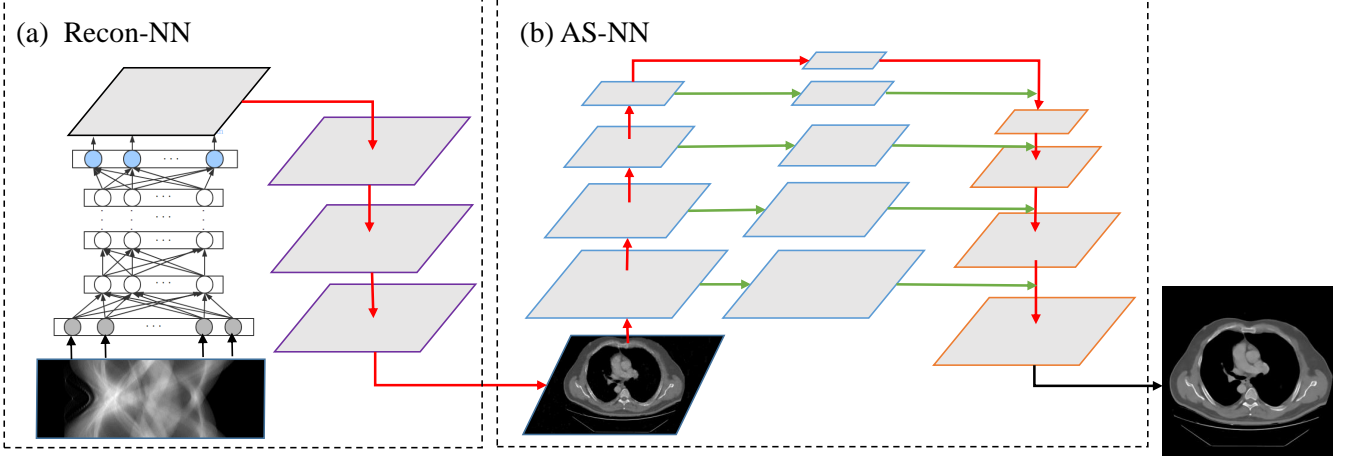


Fig. 5. The whole architecture and dataflow chart of the FAR-net, which include two parts of CT imaging processing. (a) Recon-NN for image reconstruction strategy, (b) AS-NN for artifact suppressing and de-noising.

layers. It is obviously that increasing the number of middle layers can not only accelerate convergence and improve accuracy, but also keep smoothing of loss curve.

- The results of weight matrix multiplied by matrix A ($E = W_k \cdots W_2 \cdot W_1 \cdot A$) with different parameters are shown in Fig. 7, where the dimension of A is $N = 1024$. It is illustrated that the matrix E are approximately equal to the identity matrix I (most of the nonnegative value are distributed on the diagonal).
- From the Table II, under the NMAD, it is noticed that the factorization can achieve better performance with nonnegative constraint which is a very similar conclusion with the SNMF.
- Fig. 8 shows that the variation of NMAD with the

different dimension of the matrix A . We can see that NMAD decreases as the matrix dimension increases. In fact, when the reconstructed image size is 512×512 , the dimension of matrix A can be regarded as $2^9 \times 2^9 = 2^{18}$ for reconstruction problem.

B. Sparse-views CT reconstruction

In this subsection, the FAR-net is evaluated with the medical image dataset and compared with conventional approaches for sparse-views CT.

1) *Dataset and configuration:* In the numerical experiments for sparse-views CT, we select the TCGA-ESCA cancer CT image dataset [47] as the test object. We chose 4302 images

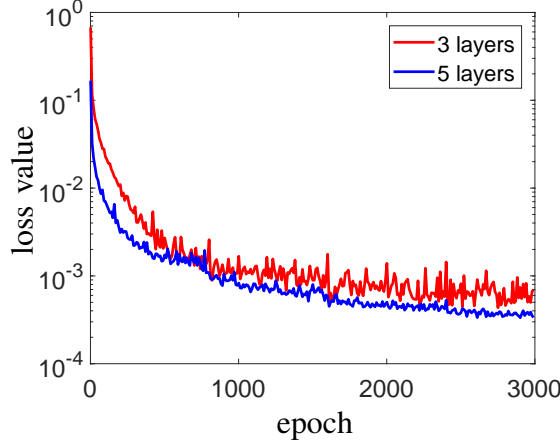


Fig. 6. MSE Loss function update with different depth of FC network. The convergence and loss value of five layers of network are significantly lower than those of three layers of network.

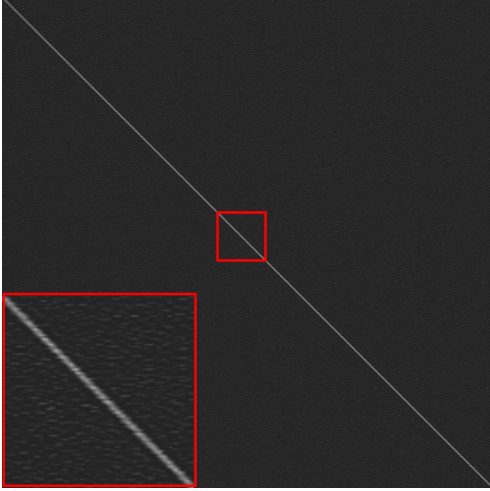


Fig. 7. A representative result of matrix multiplied by A and the inverse matrix trained by FC network. The dimension of A is 1024×1024 and display windows is $[-0.1, 0.6]$.

TABLE II
NMAD BETWEEN MATRIX E AND IDENTITY MATRIX

matrix dimension	epoch	3 layers without relu	5 layers without relu	3 layers with relu	5 layers with relu
512×512	1000	0.0331	0.0257	0.0182	0.0143
	2000	0.0294	0.0254	0.0159	0.0142
	3000	0.0280	0.0257	0.0151	0.0137
1024×1024	1000	0.0237	0.0210	0.0124	0.0114
	2000	0.0203	0.0198	0.0109	0.0108
	3000	0.0190	0.0175	0.0101	0.0099
2048×2048	1000	0.0116	0.0127	0.0067	0.0062
	2000	0.0093	0.0113	0.0061	0.0052
	3000	0.0096	0.0090	0.0052	0.0049
4096×4096	1000	0.0035	0.0034	0.0024	0.0024
	2000	0.0032	0.0032	0.0028	0.0024
	3000	0.0032	0.0032	0.0027	0.0022

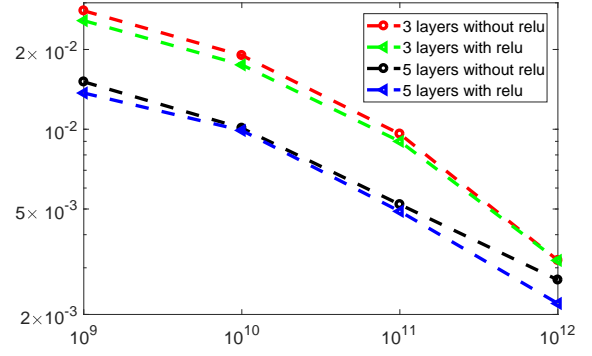


Fig. 8. The curve of NMAD between E and I with the dimension of the matrix A . The X axis represents the dimension of matrix and different curves represent different situations of networks

TABLE III
THE EXPERIMENTS CONFIGURATION OF WHOLE PROCESSING OF OUR PROPOSED NETWORK

hardware	CPU	2× E5-2620 v3
	GPU	9× NVIDIA GTX1080Ti
software	memory	512GB
	operation system	windows 10
	deep learning framework	pytorch0.4.0
hyper-parameter	GPU platform	cuda9.1, cudnn7.1
	batch size	1
	learning rate	$10^{-4} \sim 10^{-6}$
	optimizer	adam
	training iterations	600 epochs
	training time	68h35m

from the dataset with the size of 512×512 (pixels), which are regarded as the ground truth of training dataset. And the input dataset of neural network are generated by using the ground truth images to simulate parallel beam projection. The parameters of parallel beam CT projection are set as follows: the total number of views is 60, of which the interval is 3 degrees and there are 600 rays for each view. Otherwise, the testing dataset are generated in the same way and are not included in the training dataset. The configuration of whole processing of the FAR-net are displayed in Table III.

2) *results*: The images in testing dataset are predicted by the FAR-net with sparse-views projection data. For comparison, FBP algorithm, optimization-based algorithm and deep learning methods are also utilized to reconstruct images from the sparse-views projection data. In the optimization-based method, the regularization term of the objective function is the Anisotropic TV (Rudin-Osher-Fatemi model) of image and solving algorithm is Split Bregman method,

$$u = \operatorname{argmin}(|d_x u| + |d_y u| + \frac{\mu}{2} \|Au - f\|_2^2) \quad (10)$$

The regularization parameters μ for ROF is set to 100 and λ for the split-Bregman is set to 50. Moreover, U-net is chosen as deep learning based method for comparing the proposed method. The images reconstructed with sparse-view projection by FBP and the corresponding reference are set as input and label to training U-net, respectively. Hyper-parameter such as learning rate, batch size are consistent with AS-NN. In the rest of the paper, we use FBP+U-net to denote this approach.

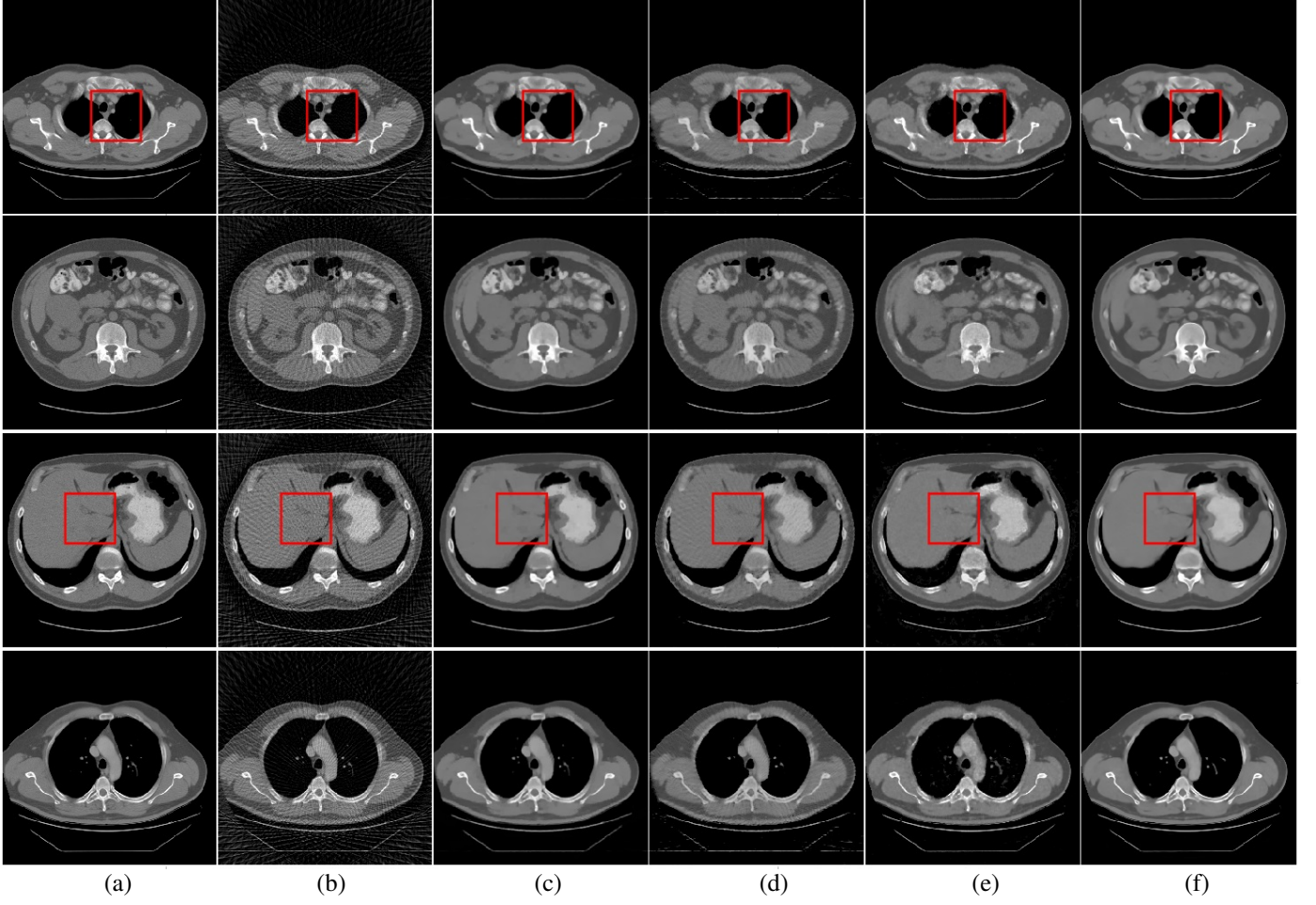


Fig. 9. Parts of reconstruction results from the test dataset without noise: (a) ground truth, (b) FBP algorithm, (c) TV based, (d) FBP+U-net, (e) Recon-NN, (f) FAR-net. The display windows are [700Hu, 1500Hu].

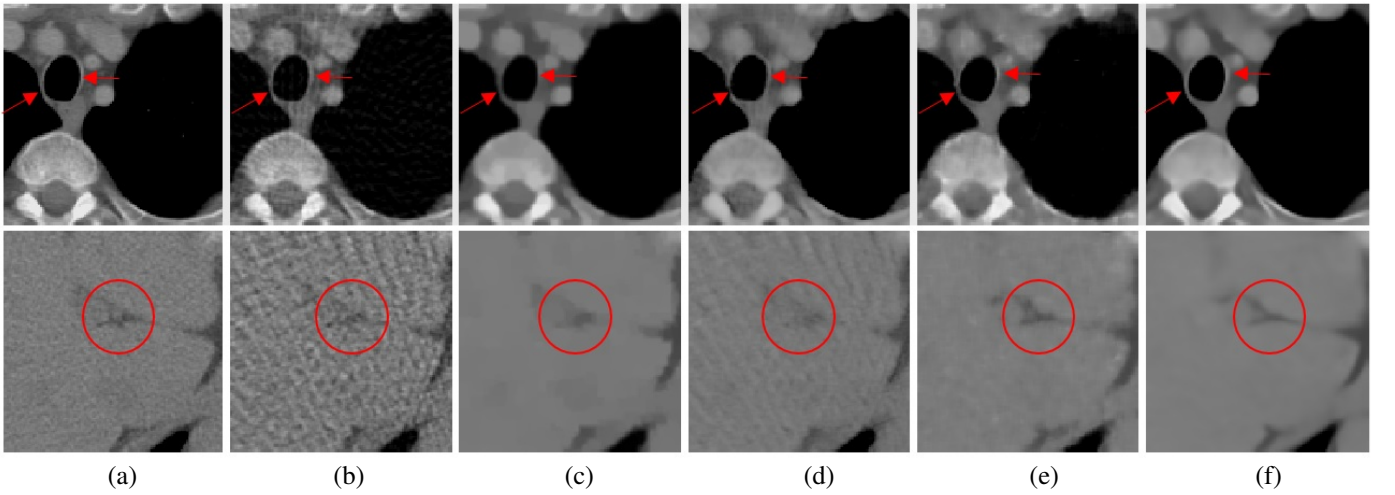


Fig. 10. Zoomed in region of interest (ROI) marked by the red box in Fig.9. (a) ground truth, (b) FBP algorithm, (c) TV based, (d) FBP+U-net, (e) Recon-NN, (f) FAR-net. The arrows indicate two locations with significant visual differences.

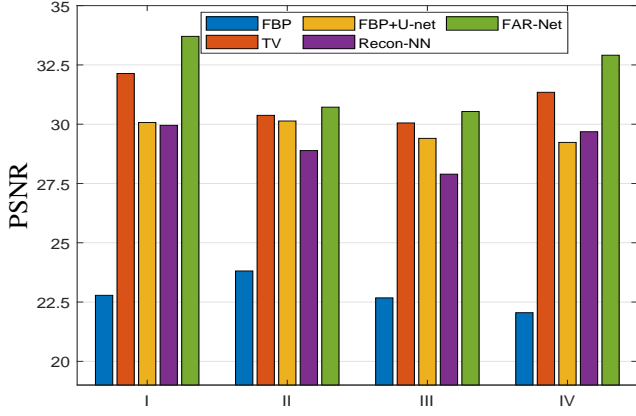


Fig. 11. PSNR performance comparison of different algorithms for the images shown in Fig.9.

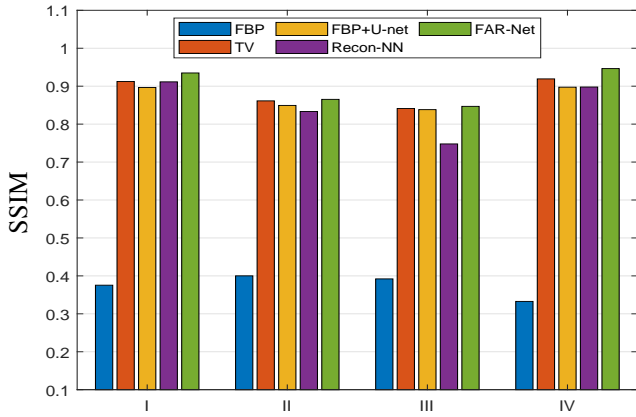


Fig. 12. SSIM performance comparison of different algorithms for the images shown in Fig.9.

Fig. 9 lists some example images which are reconstructed from 60 views with FBP, TV based method, FBP+U-net, Recon-NN and the FAR-net, respectively. It is obviously that images reconstructed from FBP suffer with heavy artifacts caused by under-sampling projection. The quality of reconstructed image is degraded by streak artifacts distributed across the whole image. All these methods suppressed image artifacts and improve image quality to various levels. The TV based method and FAR-net take more efficiently for suppressing the streak artifacts and achieving better performance in image quality. However, as shown in the Fig. 9 (c), TV based method suffered from a blocky effect and also smoothened some important small structures, such as image edge.

The example results of FBP+U-net method are shown in Fig. 9 (d). It is demonstrated that FBP+U-net removes major artifacts but some smaller streak artifacts are still available. The results of FAR-net are shown in the last column of Fig. 9. It is illustrated that the reconstruction image has no obvious blocky effect and has a best performance than other methods in low contrast region.

Fig.10 shows the zoomed in region of interest (ROI) marked by in Fig. 9. As indicated by the red arrows and circles, it is noticed that the FBP, TV based and FBP+U-net make the

edges and low contrast region blurred or distorted, where FAR-net method can still maintain the structure.

The proposed method is not only be superior to conventional method (TV based) but also better than deep learning based post-processing method (FBP+U-net). Comparing with FBP+U-net method, ours method consists of two strategies and the first strategy (Recon-NN) have obtained higher quality reconstruction results than FBP. Hence the second strategy can further obtain high quality images. The image quality indexes such as PSNR and SSIM are displayed in Fig. 11 and Fig 12, respectively. The proposed FAR-net performs the best. It is also proved that AS-NN achieves better experimental results based on better initial value mapping.

Furthermore, we test these methods in noise situations. Poisson noise specified by the incident intensity, denoted as I_0 , would always be added to the raw data, i.e.

$$p_{noisy} = -\ln\left(\frac{\text{Poissonrnd}(I_0 \times e^{-p})}{I_0}\right) \quad (11)$$

where p and p_{noisy} denote noise-free and noisy projection data, respectively. Here, we simulated Poisson noise with incident intensity $I_0 = 1.0 \times 10^6$. Fig. 13 show the results of different methods. In general, Both FBP+U-net and the FAR net are able to suppress the noise and remove the steak artifacts at the same time. However, the blocky effect is still available in the image obtained by FBP+U-net.

Fig. 14 are the regions of interest marked by red arrows and circles in Fig. 13. As indicated by the red arrows and circle, it is clearly shown that images predicated by FAR net have obvious advantages both in contrast and edge preservation. The blurred structures and over-smoothness at the edge are appeared in the images reconstructed by TV based method. For the FBP+U-net method, similar to noise free conditions, some artifacts are still remained and low contrast details are submersed. Furthermore, The above results are validated by image quality index. As shown in Fig. 15 and Fig. 16, the PSNR and SSIM are calculated. According to the results above, the proposed FAR-net can predict images with better performance both in vision and quality. Furthermore, the deep learning method has a higher efficient for image reconstruction. For example, the FAR-net only consume 0.0845 seconds to predict a image from projection data which is much less than conventional method such as TV based.

V. CONCLUSION

In this paper, we propose a neural network to map the CT reconstruction processing which is able to predict CT images from sparse-views projection data automatically. Different from most of the relevant works, which treated the neural network as black boxes, the FAR-net was directly motivated by sparseness non-negative matrix factorization and all the parameters are learned from training samples rather than pre-calculated. Furthermore, the whole net is divided into two sub structures including Recon-NN and AS-NN, which are a two-stage training strategy on single object images and multi-object images. This strategy makes the network deeper and realize a coarse-to-fine learning process and the size of whole net are optimized from $O(n^4)$ to $O(n^3)$ which could be distributed in

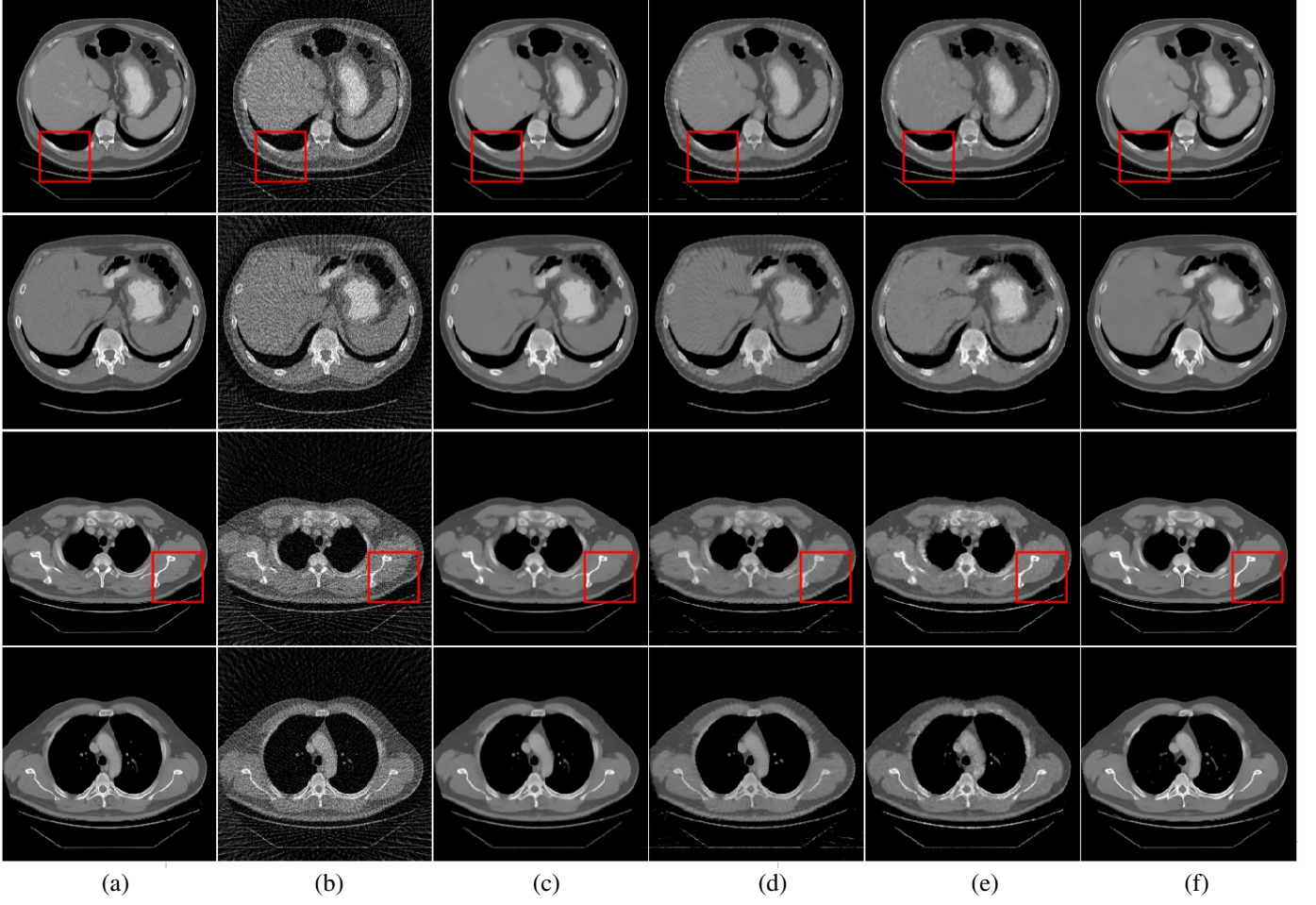


Fig. 13. Reconstruction results from the test dataset with noisy: (a) ground truth, (b) FBP algorithm, (c) TV based, (d) FBP+U-net, (e) Recon-NN, (f) FAR-net. The display windows are [700Hu, 1500Hu].

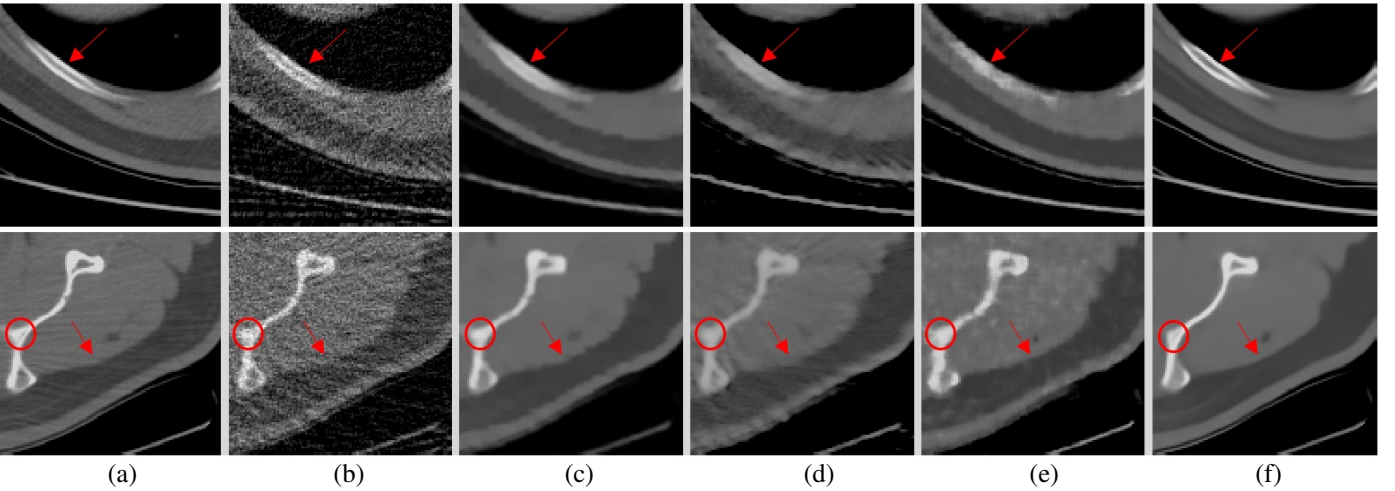


Fig. 14. Zoomed in region of interest (ROI) marked by the red box in Fig.13. (a) ground truth, (b) FBP algorithm, (c) TV based, (d) FBP+U-net, (e) Recon-NN, (f) FAR-net. The arrows indicate two locations with significant visual differences.

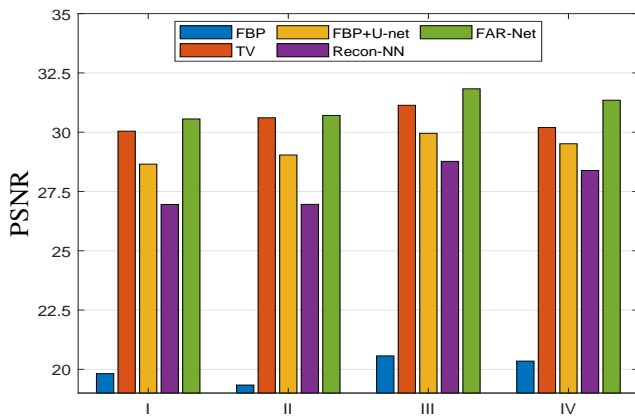


Fig. 15. PSNR performance comparison of different algorithms for the images shown in Fig.13.

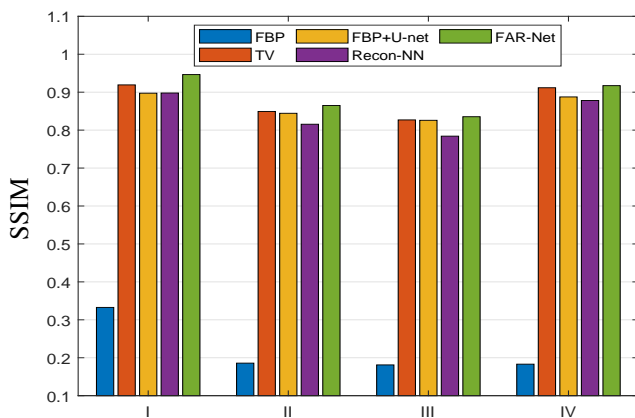


Fig. 16. SSIM performance comparison of different algorithms for the images shown in Fig.13.

a single workstation with multi-GPU. Numerical experiments show that the FAR-net can be effectively introduced into the reconstruction process and has shown the outstanding advantages in terms of noise suppression, artifact reduction, edge and feature preserving. Comparing to the conventional methods, the FAR-net has demonstrated a superior performance over in both image quality and computational efficiency.

REFERENCES

- [1] W. Zhang, H. Zhang, L. Wang, A. Cai, L. Li, and B. Yan, "Limited angle ct reconstruction by simultaneous spatial and radon domain regularization based on tv and data-driven tight frame," *Nuclear Instruments & Methods in Physics Research*, vol. 880, 2018.
- [2] R. Gordon, R. Bender, and G. T. Herman, "Algebraic reconstruction techniques (art) for three-dimensional electron microscopy and x-ray photography," *Journal of Theoretical Biology*, vol. 29, no. 3, pp. 471,IN1,477–476,IN2,481, 1970.
- [3] A. H. Andersen and A. C. Kak, "Simultaneous algebraic reconstruction technique (sart): A superior implementation of the art algorithm," *Ultrason Imaging*, vol. 6, no. 1, pp. 81–94, 1984.
- [4] A. P. Dempster, "Maximum likelihood from incomplete data via the em algorithm (with discussion)," *Journal of the Royal Statistical Society: Series B*, vol. 39, 1977.
- [5] D. L. Donoho, "Compressed sensing," *IEEE Transactions on Information Theory*, vol. 52, no. 4, pp. 1289–1306, 2006.
- [6] E. Y. Sidky and X. Pan, "Image reconstruction in circular cone-beam computed tomography by constrained, total-variation minimization," *Physics in Medicine & Biology*, vol. 53, no. 17, p. 4777, 2008.

- [7] Y. Zhang, W. Zhang, Y. Lei, and J. Zhou, "Few-view image reconstruction with fractional-order total variation," *J Opt Soc Am A Opt Image Sci Vis*, vol. 31, no. 5, pp. 981–995, 2014.
- [8] Y. Zhang, Y. Wang, W. Zhang, F. Lin, Y. Pu, and J. Zhou, "Statistical iterative reconstruction using adaptive fractional order regularization," *Biomedical Optics Express*, vol. 7, no. 3, pp. 1015–1029, 2016.
- [9] Y. Zhang, W. H. Zhang, H. Chen, M. L. Yang, T. Y. Li, and J. L. Zhou, "Few-view image reconstruction combining total variation and a high-order norm," *International Journal of Imaging Systems & Technology*, vol. 23, no. 3, pp. 249–255, 2013.
- [10] Q. Xu, H. Yu, X. Mou, L. Zhang, H. Jiang, and G. Wang, "Low-dose x-ray ct reconstruction via dictionary learning," *IEEE Transactions on Medical Imaging*, vol. 31, no. 9, pp. 1682–1697, 2012.
- [11] Y. Chen, D. Gao, C. Nie, L. Luo, W. Chen, X. Yin, and Y. Lin, "Bayesian statistical reconstruction for low-dose x-ray computed tomography using an adaptive-weighting nonlocal prior," *Computerized Medical Imaging & Graphics the Official Journal of the Computerized Medical Imaging Society*, vol. 33, no. 7, pp. 495–500, 2009.
- [12] M. Jianhua, Z. Hua, G. Yang, H. Jing, L. Zhengrong, F. Qianjing, and C. Wufan, "Iterative image reconstruction for cerebral perfusion ct using a pre-contrast scan induced edge-preserving prior," *Physics in Medicine & Biology*, vol. 57, no. 22, p. 7519, 2012.
- [13] Y. Zhang, Y. Xi, Q. Yang, W. Cong, J. Zhou, and G. Wang, "Spectral ct reconstruction with image sparsity and spectral mean," *IEEE Transactions on Computational Imaging*, vol. 2, no. 4, pp. 510–523, 2016.
- [14] S. Verma and N. Khare, "Denoising of computed tomography images using wavelet transform," *International Journal for Innovative Research in Science & Technology*, 2015.
- [15] F. Kallel, M. Sahnoun, A. B. Hamida, and K. Chtourou, "Ct scan contrast enhancement using singular value decomposition and adaptive gamma correction," *Signal Image & Video Processing*, no. 3, pp. 1–9, 2018.
- [16] Q. Wang, Y. Zhu, and H. Li, "Local linear constraint based optimization model for dual spectral ct," in *The 14th international Meeting on fully three-dimensional image reconstruction in radiology and nuclear medicine*, 2017, pp. 352–358. [Online]. Available: 10.1088/1361-6560/aa8e13
- [17] Cuda accelerated computing homepage. [Online]. Available: <https://developer.nvidia.com/deep-learning>
- [18] K. Zhang, W. Zuo, S. Gu, and L. Zhang, "Learning deep cnn denoiser prior for image restoration," *CVPR*, pp. 2808–2817, 2017.
- [19] K. Yu, C. Dong, L. Lin, and C. C. Loy, "Crafting a toolchain for image restoration by deep reinforcement learning," *CoRR*, vol. abs/1804.03312, 2018. [Online]. Available: <http://arxiv.org/abs/1804.03312>
- [20] Y. Zhang and H. Yu, "Convolutional neural network based metal artifact reduction in x-ray computed tomography," *IEEE Transactions on Medical Imaging*, vol. PP, no. 99, pp. 1–1, 2017.
- [21] L. Gjestebj, Q. Yang, Y. Xi, H. Shan, B. Claus, Y. Jin, B. De Man, and G. Wang, "Deep learning methods for ct image-domain metal artifact reduction," in *Society of Photo-Optical Instrumentation Engineers*, 2017, p. 31.
- [22] H. Chen, Y. Zhang, M. K. Kalra, F. Lin, Y. Chen, P. Liao, J. Zhou, and G. Wang, "Low-dose ct with a residual encoder-decoder convolutional neural network (red-cnn)," *IEEE Transactions on Medical Imaging*, no. 99, pp. 1–1, 2017. [Online]. Available: 10.1109/TMI.2017.2715284
- [23] E. Kang, J. Min, and J. C. Ye, "A deep convolutional neural network using directional wavelets for low-dose x-ray ct reconstruction," *Medical Physics*, vol. 44, no. 10, p. e360, 2017. [Online]. Available: arXiv:1610.09736v3
- [24] H. Chen, Y. Zhang, W. Zhang, P. Liao, K. Li, J. Zhou, and G. Wang, "Low-dose ct via convolutional neural network," *Biomedical Optics Express*, vol. 8, no. 2, p. 679, 2017.
- [25] Q. Yang, P. Yan, Y. Zhang, H. Yu, Y. Shi, X. Mou, M. K. Kalra, and G. Wang, "Low dose CT image denoising using a generative adversarial network with wasserstein distance and perceptual loss," *CoRR*, vol. abs/1708.00961, 2017. [Online]. Available: <http://arxiv.org/abs/1708.00961>
- [26] Y. Han and J. C. Ye, "Framing u-net via deep convolutional framelets: Application to sparse-view ct," *IEEE Transactions on Medical Imaging*, 2017. [Online]. Available: arXiv:1708.08333v2
- [27] W. Zhang, H. Zhang, L. Wang, X. Wang, A. Cai, L. Li, T. Niu, and B. Yan, "Image domain dual material decomposition for dual-energy ct using butterfly network," *CVPR*, 2018.
- [28] H. Chen, Y. Zhang, Y. Chen, J. Zhang, W. Zhang, H. Sun, Y. Lv, P. Liao, J. Zhou, and G. Wang, "Learn: Learned experts assessment-based reconstruction network for sparse-data ct," *IEEE Transactions on Medical Imaging*, vol. 37, no. 6, pp. 1333–1347, June 2018.

- [29] K. Gong, J. Guan, K. Kim, X. Zhang, G. Fakhri, J. Qi, and Q. Li, "Iterative pet image reconstruction using convolutional neural network representation," *IEEE Transactions on Medical Imaging*, 10 2017.
- [30] G. Wang, "A perspective on deep imaging," *IEEE Access*, vol. 4, pp. 8914–8924, 2016.
- [31] M. Y. Liu, T. Breuel, and J. Kautz, "Unsupervised image-to-image translation networks," *CORR*, 2017. [Online]. Available: arXiv:1703.00848
- [32] Z. Yi, H. Zhang, P. Tan, and M. Gong, "Dualgan: Unsupervised dual learning for image-to-image translation," in *IEEE International Conference on Computer Vision*, 2017, pp. 2868–2876. [Online]. Available: arXiv:1704.02510
- [33] T. Wrfl, F. C. Ghesu, V. Christlein, and A. Maier, "Deep learning computed tomography," in *International Conference on Medical Image Computing and Computer-Assisted Intervention*, 2016.
- [34] B. Zhu, J. Z. Liu, S. F. Cauley, B. R. Rosen, and M. S. Rosen, "Image reconstruction by domain-transform manifold learning," *Nature*, vol. 555, no. 7697, p. 487, 2018.
- [35] Y. Li, K. Li, C. Zhang, J. Montoya, and G. Chen, "Learning to reconstruct computed tomography (ct) images directly from sinogram data under a variety of data acquisition conditions," *IEEE Transactions on Medical Imaging*, pp. 1–1, 2019.
- [36] P. O. Hoyer, "Non-negative matrix factorization with sparseness constraints," *Journal of machine learning research*, vol. 5, no. Nov, pp. 1457–1469, 2004.
- [37] D. D. Lee and H. S. Seung, "Learning the parts of objects by non-negative matrix factorization," *Nature*, vol. 401, no. 6755, p. 788, 1999.
- [38] —, "Algorithms for non-negative matrix factorization," in *Advances in Neural Information Processing Systems 13*, T. K. Leen, T. G. Dietterich, and V. Tresp, Eds. MIT Press, 2001, pp. 556–562. [Online]. Available: <http://papers.nips.cc/paper/1861-algorithms-for-non-negative-matrix-factorization.pdf>
- [39] Y. Zhao, X. Zhao, and P. Zhang, "An extended algebraic reconstruction technique (e-art) for dual spectral ct," *IEEE Trans Med Imaging*, vol. 34, no. 3, pp. 761–768, 2015.
- [40] R. Girshick, "Fast r-cnn," *Computer Science*, 2015. [Online]. Available: arXiv:1504.08083v2
- [41] W. Liu, D. Anguelov, D. Erhan, C. Szegedy, S. Reed, C. Y. Fu, and A. C. Berg, "Ssd: Single shot multibox detector," in *European Conference on Computer Vision*, 2016, pp. 21–37.
- [42] S. Jegou, M. Drozdal, D. Vazquez, A. Romero, and Y. Bengio, "The one hundred layers tiramisu: Fully convolutional densenets for semantic segmentation," *CoRR*, vol. abs/1611.09326, 2016. [Online]. Available: <http://arxiv.org/abs/1611.09326>
- [43] O. Ronneberger, P. Fischer, and T. Brox, "U-net: Convolutional networks for biomedical image segmentation," *CoRR*, vol. abs/1505.04597, 2015. [Online]. Available: <http://arxiv.org/abs/1505.04597>
- [44] K. He, X. Zhang, S. Ren, and J. Sun, "Deep residual learning for image recognition," *IEEE Conference on Computer Vision and Pattern Recognition*, vol. abs/1512.03385, 2015. [Online]. Available: <http://arxiv.org/abs/1512.03385>
- [45] G. Huang, Z. Liu, and K. Q. Weinberger, "Densely connected convolutional networks," *CoRR*, vol. abs/1608.06993, 2016. [Online]. Available: <http://arxiv.org/abs/1608.06993>
- [46] The pascal visual object classes homepage. [Online]. Available: <http://host.robots.ox.ac.uk/pascal/VOC/>
- [47] "Tcga-esca." [Online]. Available: <http://datajcu.cn/Datajcu/web/datasetInstanceDetail/448>